RSC Advances

PAPER

View Article Online
View Journal | View Issue

Cite this: *RSC Adv.*, 2019, **9**, 23979

Structural characterization of an amorphous VS_4 and its lithiation/delithiation behavior studied by solid-state NMR spectroscopy†

Keiji Shimoda, *[a] Kazuto Koganei,[b] Tomonari Takeuchi,[b] Toshiyuki Matsunaga,[a] Miwa Murakami,[a] Hikari Sakaebe, [b] Hironori Kobayashi[b] and Eiichiro Matsubara[c]

Received 10th June 2019
Accepted 29th July 2019

DOI: 10.1039/c9ra04338a

rsc.li/rsc-advances

Vanadium sulfide (VS_4) is one of the promising positive electrode materials for next-generation rechargeable lithium-ion batteries because of its high theoretical capacity (1196 mA h g^{-1}). Crystalline VS_4 has a unique structure, in which the Peierls-distorted one-dimensional chains of V–V bonds along the *c* axis are loosely connected to each other through van der Waals interactions. In this study, an amorphous VS_4 is prepared by mechanical milling of the crystalline material, and its lithiation/delithiation behavior is investigated by solid-state nuclear magnetic resonance (NMR) spectroscopy. The amorphous VS_4 shows a chain structure similar to that of crystalline VS_4. The amorphous host structure is found to change drastically during the lithiation process to form Li_3VS_4: the V ions become tetrahedrally coordinated by S ions, in which the valence states of V and S ions simultaneously change from V^{4+} to V^{5+} and S^- to S^{2-}, respectively. When the Li insertion proceeds further, the valence state of V ions is reduced. After the 1st cycle, the amorphous VS_4 recovers to the chain-like structure although it is highly disordered. No conversion to elemental V is observed, and a high capacity of 700 mA h g^{-1} is reversibly delivered between 1.5 and 2.6 V.

1. Introduction

Elemental sulfur is one of the most promising electrode materials for next-generation rechargeable lithium-ion batteries, because of its high theoretical capacity of 1672 mA h g^{-1}. Its corresponding electrochemical reaction can be expressed as $S + 2Li^+ + 2e^- = Li_2S$, and involves the S^0/S^{2-} redox couple at an average potential of 2.15 V *vs.* Li/Li^+.[1] However, two well-known problems have yet to be solved. The first is that both S and Li_2S are electronically resistive, which gives rise to relatively poor electrochemical performance in practical applications. The other problem is the dissolution of lithium polysulfide intermediates Li_2S_x ($2 < x < 8$) in nonaqueous electrolyte solutions during the charge–discharge cycles, leading to capacity fading.[1–3]

To enhance the electronic conductivity of S, composite electrodes with carbonaceous materials have been developed, and excellent electrochemical properties were reported for a highly ordered nanostructured carbon–sulfur composite electrode.[4–6] As an alternative approach, considerable attention has been paid to transition metal (TM) sulfides, such as TiS_2, FeS_2, and MoS_2,[7–16] which have been examined as positive or negative electrode materials for conventional lithium-ion batteries. TM sulfide-based positive electrodes were introduced for Li–S batteries, in which the TM ions were considered to act merely as electron conductive agents. New sulfur-rich electrode materials based on TM sulfides have been developed in recent years.[17–23] For example, amorphous TiS_4 was synthesized as a cathode material by a mechanochemical process from a TiS_2 and S mixture and showed a stable charge–discharge profile in a nonaqueous electrolyte solution.[17] An Fe-doped Li_2S-based material, Li_8FeS_5, showed a high discharge capacity close to 730 mA h g^{-1}.[21] These studies suggest that the formation of metal–sulfur bonds is important to suppress polysulfide dissolution.

Vanadium sulfide (VS_4, mineral name: patronite) has a unique crystalline form, in which infinite chains of V–V bonds along the *c* axis show Peierls distortion with alternate V–V distances of 2.83 and 3.22 Å, and each V ion is coordinated by 4 disulfide anions $[S_2]^{2-}$.[24] Initial discharge and charge capacities of the crystalline VS_4 (c-VS_4) electrode composite with reduced graphene oxide (VS_4-rGO) were reported to be 1669 and 1105 mA h g^{-1} at a current rate of 0.1C, and an excellent charge capacity retention of 954 mA h g^{-1} was obtained after 100 cycles.[25] Good capacity retention at high current rates was also

---

[a] *Office of Society-Academia Collaboration for Innovation, Kyoto University, Gokasho, Uji, Kyoto 611-0011, Japan. E-mail: k-shimoda@saci.kyoto-u.ac.jp; Fax: +81-774-38-4996; Tel: +81-774-38-4967*

[b] *National Institute of Advanced Industrial Science and Technology, Ikeda, Osaka 563-8577, Japan*

[c] *Department of Materials Science and Engineering, Kyoto University, Kyoto 606-8501, Japan*

† Electronic supplementary information (ESI) available. See DOI: 10.1039/c9ra04338a

demonstrated.[25,26] The charge–discharge mechanism of the c-VS_4 electrode was carefully studied by pair distribution function (PDF) analysis of synchrotron-radiation X-ray scattering data and X-ray absorption near-edge spectroscopy (XANES) as well as X-ray diffraction (XRD):[27] *in situ* XRD measurements showed that c-VS_4 started to transform into a highly disordered or amorphous phase from the beginning of lithiation. The results of X-ray PDF and S K-edge XANES analyses suggest the breaking of S–S dimers accompanied by the formation of $[VS_4]^{3-}$ tetrahedral units during lithiation, and the subsequent formation of face-centered cubic (fcc) V and Li_2S at the end of discharge at 0 V.[27] These reactions were proved to be partially reversible, in contrast with the previous speculation that the formed V is inactive and Li_2S is reversibly delithiated/lithiated.[26] Solid-state nuclear magnetic resonance (NMR) was also successfully applied to understand the structural changes around Li and V ions during the lithiation/delithiation process:[27] the ^{51}V signal of c-VS_4 disappeared and metallic V and Li_2S were observed during the lithiation. Recently, our group examined the charge–discharge properties of the c-VS_4 electrode without rGO in a potential window between 1.0 and 3.0 V.[28] The conversion to elemental V was not observed within this potential window, and the pristine VS_4-like local structure, although non-crystalline, was recovered after the initial charge–discharge cycle. Moreover, it was found that c-VS_4 transforms into an amorphous phase by mechanical milling.[29] The charge–discharge profile of the amorphous VS_4 (a-VS_4) resembles that of c-VS_4, and its electrochemical properties were moderately improved.[29] However, the exact structural information of the pristine a-VS_4 and its charge–discharge mechanism are still unclear. As shown in a previous study,[27] NMR is a suitable technique to characterize the framework structure of V ions as well as the non-framework environment of labile Li ions. Therefore, in the present study, we investigate the structure of an amorphous VS_4 and its changes during the lithiation/delithiation process using solid-state NMR spectroscopy.

2. Experimental

Crystalline VS_4 was first synthesized without rGO from a mixture of V_2S_3 (99%, Kojundo Chemical Laboratory) and S (99.9%, Wako) in a molar ratio of 1 : 6, which was sealed in a glass tube under vacuum and heated two times at 400 °C for 12 h.[28] After cooling to room temperature, excessive sulfur was removed by annealing at 200 °C under vacuum. Then, the amorphous VS_4 was prepared from the sintered sample by mechanical milling for 40 h at 270 rpm in a planetary ball mill (Pulverisette 7, Fritsch). The working electrode consisted of a mixture of the active material (a-VS_4), Ketjen Black (KB), and polytetrafluoroethylene (PTFE) binder in a weight ratio of 59 : 29 : 12 on a Ni mesh current collector. A Li foil (0.2 mm in thickness, >99.9%, Honjo Metal) was used as the negative electrode, and a microporous polyolefin sheet was chosen as the separator. A solution of 1 M $LiPF_6$ dissolved in a 1 : 1 volume ratio mixture of ethylene carbonate (EC) and dimethyl carbonate (DMC) was used as the electrolyte solution (Tomiyama Pure Chemical Industries, battery grade). Coin-type or laminate-type cells were assembled in an Ar-filled glove box. The electrochemical measurements were performed at 30 °C. The cells were galvanostatically cycled between 1.5 and 2.6 V at a current density of 59.8 mA g^{-1} (0.05C rate) using a TOSCAT-3100 battery-testing system (Toyo System). They were then carefully disassembled at selected discharge/charge states in the glove box and rinsed with DMC to remove the residual electrolyte solution.

XRD measurements were carried out for sealed samples on a D8 ADVANCE X-ray diffractometer (Bruker AXS) with a Cu K_α source and a SmartLab diffractometer (Rigaku) with a Mo K_α source. Raman spectra were acquired using a LabRAM HR-800 spectrometer (Horiba-Jobin Yvon) with a 50× lens, 600 and 1800 grooves per mm grating, and an excitation wavelength of 632.8 nm (He–Ne laser). The electrode samples were sealed in transparent gas-barrier films. The laser power was reduced to less than 1 mW to avoid laser-induced degradation on the targeted particles. The exposure time was 10 s × 10 times on more than ten different particles. XPS measurements were performed on a PHI5000 VersaProbe II (ULVAC-PHI) photoelectron spectrometer with monochromatic Al K_α radiation (1486.6 eV). The samples were transferred to an ultra-high vacuum sample chamber ($<4 \times 10^{-7}$ Pa) without exposing them to air. The pass energy was set to 23.5 eV. Dual-beam charge neutralization (simultaneous irradiation with low-energy electrons and Ar^+ ion beams) was applied to suppress sample charging. The spectra were acquired without Ar^+ ion sputtering to avoid sample damage. The binding energies were calibrated with respect to the C 1s signal from KB at 284.6 eV.

NMR spectra were acquired on a DD2 600 spectrometer (Agilent Technologies) at a magnetic field of 14.1 T. Operando ^7Li NMR measurements were performed with a homemade wide-bore static probe, in which a flat laminate-type cell was placed in the center of a 10 mm-diameter solenoid coil. A Hahn echo pulse sequence was used, with a first pulse width of 4.5 μs and an echo decay of 8 μs. Each spectrum was averaged over 30 min (scan number of 1792 with a relaxation delay of 1 s). ^7Li and ^{51}V magic-angle spinning (MAS) NMR spectra were acquired with a wide-bore T3 MAS probe (Agilent Technologies). Powder samples were packed into 1.2 mmϕ MAS ZrO_2 rotors with airtight caps in an Ar-filled glove box and spun at a rate of 60 kHz during the measurements. A rotor-synchronized Hahn echo pulse sequence ($\pi/2$-τ-π-τ-acq) was used with a $\pi/2$ pulse width of 1.0 μs and a relaxation delay of 5 s for ^7Li measurements (longer delay for a full signal detection including byproduct components), and 0.5 μs and 0.5 s for ^{51}V measurements, respectively. All spectra were referenced to 1 M LiCl solution at 0.0 ppm and V_2O_5 at −612 ppm (a secondary solid reference relative to neat $VOCl_3$ at 0.0 ppm) for ^7Li and ^{51}V measurements, respectively.

3. Results and discussion

3.1. Structural characterization of a-VS_4

Fig. 1a compares the XRD profiles of c-VS_4 and a-VS_4. The diffraction pattern of c-VS_4 prepared in this study was indexed to the space group *C*2/*c*, which was recently revised against *I*2/*c*,

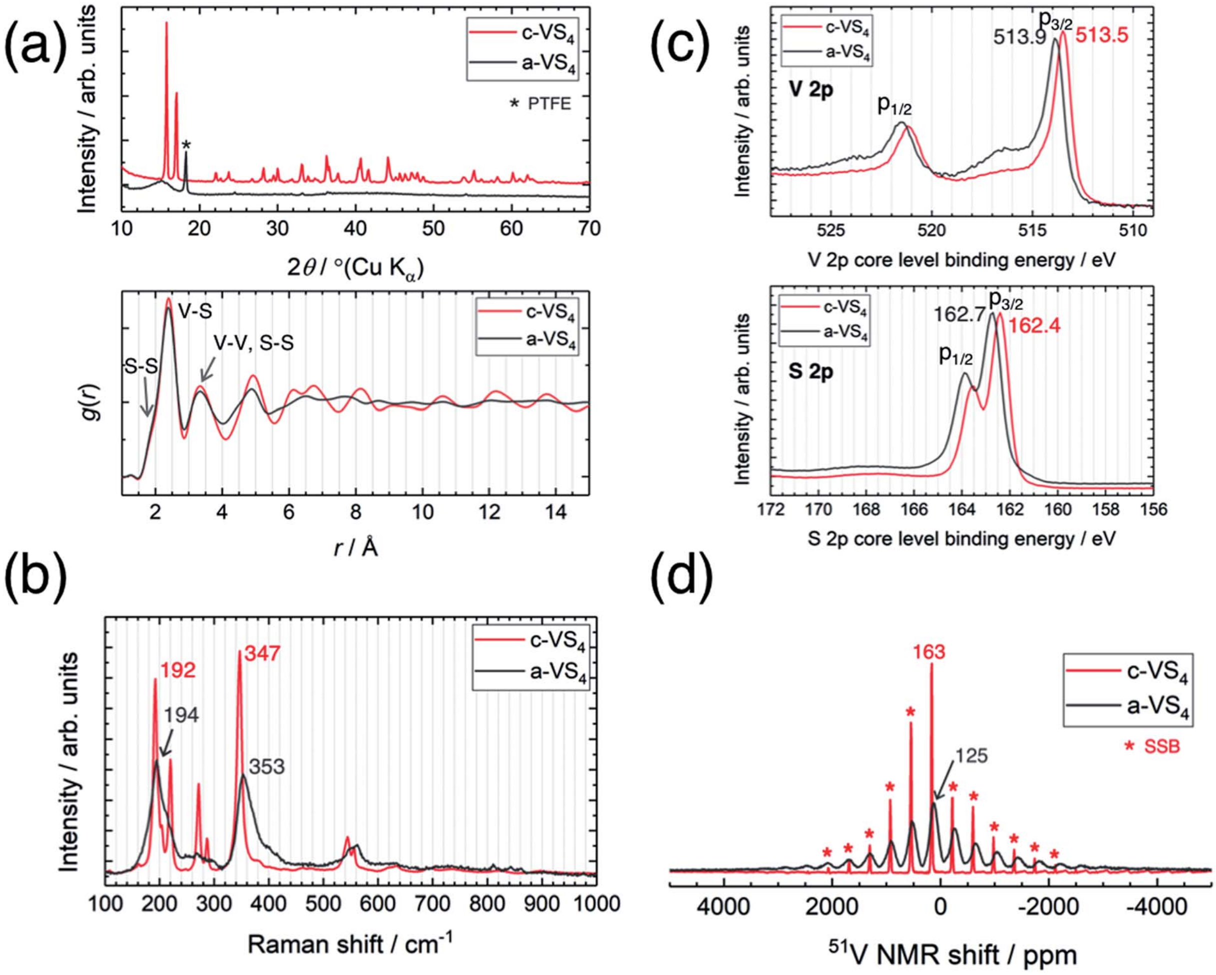

Fig. 1 Comparison between crystalline and amorphous VS_4. (a) XRD profiles (upper panel) and PDF patterns (lower panel), (b) Raman spectra, (c) XPS spectra, and (d) ^{51}V MAS NMR spectra.

as reported previously.[24,30] The diffraction peaks disappeared after mechanical milling of c-VS_4, and a broad halo was observed at ~15°. This indicates mechanochemical amorphization of the VS_4 crystal structure (*i.e.*, a-VS_4). We note that the crystalline component started to decrease after the mechanical milling of 10 h and completely disappeared with the milling time of up to 40 h. Needle-shaped particles characteristic of c-VS_4 was completely broken and pulverized on the scanning electron microscope (SEM) images (not shown). The amorphous structure of a-VS_4 was examined by X-ray PDF analysis using a Mo K_α source (Fig. 1a, lower panel). The interatomic distances in $g(r)$ functions of c-VS_4 and a-VS_4 were similar to each other up to 5 Å: a shoulder at ~2.0 Å and a peak at 2.4 Å are assigned to S–S distance in a disulfide bond and V–S distance, respectively. A longer V–V distance in the Peierls-distorted chain and a second-neighbor S–S distance are merged at 3.3 Å. This indicates that the local structure of a-VS_4 resemble that of c-VS_4.

The Raman spectra of c-VS_4 and a-VS_4 are shown in Fig. 1b. First, we obtained a high-quality and high-resolution spectrum for c-VS_4 using reduced laser power. Intense peaks were observed at 192, 220, 272, 287, 347, 544, and 555 cm^{-1}. We confirmed that these vibrational peaks arise from c-VS_4 based on the theoretical calculation of Raman-active frequencies and intensities (Fig. S1†). The Raman spectrum of a-VS_4 shows broader features than that of c-VS_4, proving a similar structural unit with local disorder. Two intense bands at 194 and 353 cm^{-1} and a weaker band at ~560 cm^{-1} are attributed to V–S bond stretching mode, breathing motion of the V_2S_4 cage, and S–S bond stretching/twisting, respectively.[31]

The V 2p and S 2p XPS spectra of c-VS_4 and a-VS_4 are compared in Fig. 1c. The V 2p core-level spectra are split into two components, $p_{3/2}$ and $p_{1/2}$, due to spin–orbit coupling. The V $2p_{3/2}$ peak position of a-VS_4 (513.9 eV) is close to that of c-VS_4 (513.5 eV), which is attributed to the V^{4+} valence state (514.1 eV in ref. 32). Similarly, the S 2p core-level spectra show a doublet peak, $p_{3/2}$ and $p_{1/2}$ with an intensity ratio of 2 : 1, due to spin–orbit coupling. The S $2p_{3/2}$ peak position of a-VS_4 (162.7 eV) is close to that of c-VS_4 (162.4 eV), which is assigned to the S^- (or $[S_2]^{2-}$) state.[32,33] Therefore, the valence state of a-VS_4 is almost the same as that of c-VS_4. In addition, the S/V atomic ratios of c- and a-VS_4 were estimated to be 4.0(1) and 3.7(1), respectively.

Fig. 1d shows the ^{51}V MAS NMR spectra of c-VS$_4$ and a-VS$_4$. The spectrum of c-VS$_4$ shows a sharp signal at 163 ppm with significant spinning sideband manifolds (SSBs). It is important to note that the valence state of V^{4+} in c-VS$_4$ is expected to be paramagnetic (the 3d^1 electronic configuration). However, if it is indeed paramagnetic, the ^{51}V signal would be almost undetectable due to ultrafast relaxation of free induction decay (FID). The one-dimensional linear chain structure of c-VS$_4$ is stabilized by Peierls distortion, which gives rise to alternating short and long V–V distances.[27] Electronic spin-pairing occurs within the short V–V bond, resulting in a diamagnetic shift in the ^{51}V spectrum.[27] The spectrum of a-VS$_4$ shows a relatively broad signal at 125 ppm with significant SSBs. The isotropic shift of a-VS$_4$ is close (but not equal) in position to that of c-VS$_4$, suggesting that a-VS$_4$ also has the Peierls-distorted chain structure with some configuration disordering.

3.2. Structural changes during charge–discharge cycling

Fig. 2 shows the charge–discharge profile of the Li//a-VS$_4$ cell. The initial discharge capacity at 1.5 V was ~750 mA h g^{-1} (Fig. S2†), corresponding to the average composition of Li$_5$VS$_4$. It should be noted that the theoretical capacity of 1196 mA h g^{-1} ($VS_4 + 8Li^+ + 8e^- = V + 4Li_2S$) is achieved at a voltage below 0.5 V.[25–27] Within the potential window in the present study, a plateau-like feature was observed. The XRD profiles showed that the lithiated/delithiated a-VS$_4$ samples preserved the amorphous structure (Fig. S3†). Structural evaluation of these materials is currently in progress using synchrotron-radiation X-ray PDF analysis.[29]

To understand the lithiation/delithiation behavior of a-VS$_4$, operando ^{7}Li NMR measurements were carried out (Fig. 3). Two signals were observed before the electrochemical test. The sharp peaks at ~0 and 275 ppm originate from the LiPF$_6$ salt in the electrolyte solution and the Li metal used as the counter electrode, respectively. During the lithiation process, the ^{7}Li signal from the Li ions inserted in a-VS$_4$ (*i.e.*, a-Li$_x$VS$_4$) increased in intensity, which gives rise to a broad signal centered at ~25 ppm. The spectral evolution changed with an increase in Li content above Li$_{\sim3.6}$VS$_4$: the a-Li$_x$VS$_4$ signal shifted to higher frequencies with a significant increase in width. This is followed by a decrease in the integrated intensity of the a-Li$_x$VS$_4$ signal after the measurement time of 15 h. The intensity loss may be attributed to the incomplete detection of the broader signal component. These results indicate an increasing dipolar interaction between the ^{7}Li nuclei and the unpaired electrons on the V ions during the latter half of the discharge process. Similar behavior was observed in the previous study.[34] On the subsequent charge process, the integrated intensity of the a-Li$_x$VS$_4$ signal first increased and then decreased. The spectral changes were basically reversible (see also Fig. S4†).

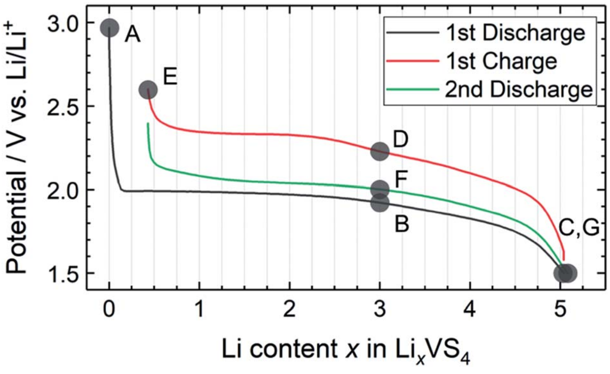

Fig. 2 Charge–discharge profile of the Li//a-VS$_4$ cell between 1.5 and 2.6 V. Sampling points are marked on the figure.

Fig. 4 shows high-resolution ^{7}Li and ^{51}V MAS NMR spectra for the electrode samples disassembled at the points shown in Fig. 2. The spectra were normalized by the scan number and sample weight in the rotors. The pristine a-VS$_4$ has no signal in the ^{7}Li MAS spectrum as expected (spectrum A in Fig. 4a), but the lithiated samples showed a sharp peak at 0 ppm, indicating the diamagnetic nature of the a-Li$_x$VS$_4$ signal (B, C, D, F, G). Based on the operando ^{7}Li spectral evolution and ^{51}V MAS NMR spectra discussed later, the signal at 0 ppm was attributed to a diamagnetic V^{5+}-containing material, most probably a-Li$_3$VS$_4$, as had been suggested in a previous study.[27] Another shoulder peak at ~5 ppm for the samples at the midpoint of the charge–discharge process (B, D, F) may be attributed to the a-Li$_{3+d}$VS$_4$ intermediate material.[27] A broad signal centered at ~20 ppm was observed at 1.5 V (C), which is clearly affected by the hyperfine interactions between Li ions and paramagnetic ions, indicating the formation of V^{4+} and/or V^{3+} species in a-Li$_{3+d'}$VS$_4$.[27] This corresponds to the signal broadening and intensity loss observed in the operando measurements. Small peaks were also observed at 2.0 and 2.6 ppm at 1.5 V (C, G), one of which may be associated with the formation of Li$_2$S.[27] The spectral changes were reversible.

The pristine a-VS$_4$ shows an isotropic ^{51}V signal at 125 ppm with significant SSBs (A in Fig. 4b). A new peak was clearly observed at 1420 ppm for the a-Li$_x$VS$_4$ samples (B, C, D, F, G). This chemical shift is close to that of K$_3$VS$_4$ (1375 ppm),[27] in which the V^{5+} ions are tetrahedrally coordinated by S^{2-} ions.[35] Therefore, it is ascribed to a-Li$_3$VS$_4$. We emphasize that the formation of the [VS$_4$]$^{3-}$ tetrahedral structure was explicitly demonstrated in the present ^{51}V MAS NMR spectra compared to the previous study.[27] Both the signals from a-VS$_4$ and a-Li$_3$VS$_4$ were observed for the samples at the midpoint of the charge–discharge process (B, D, F). This suggests a two-phase reaction process between a-VS$_4$ and a-Li$_3$VS$_4$, in agreement with the flat voltage in this region (Fig. 2). At 1.5 V (C, G), the a-VS$_4$ signal almost disappeared, and a weak signal at ~830 ppm was identified. The latter signal may come from the V^{5+} ions close to the paramagnetic V^{4+} and/or V^{3+} ions in a-Li$_{3+d'}$VS$_4$, which is affected by the hyperfine interactions. We did not find the ^{51}V signal from metallic V at ~5500 ppm with a carrier frequency at 5500 ppm, in contrast to the previous study.[27] Therefore, we believe that the conversion reaction to elemental V starts at a potential below 1.5 V. The a-Li$_3$VS$_4$ signal disappeared, and a broad signal at ~120 ppm was recovered after full delithiation (E). The latter signal was attributed to a-VS$_4$, but its intensity was significantly reduced compared to the pristine material (A). This intensity reduction is probably due to the increasing local

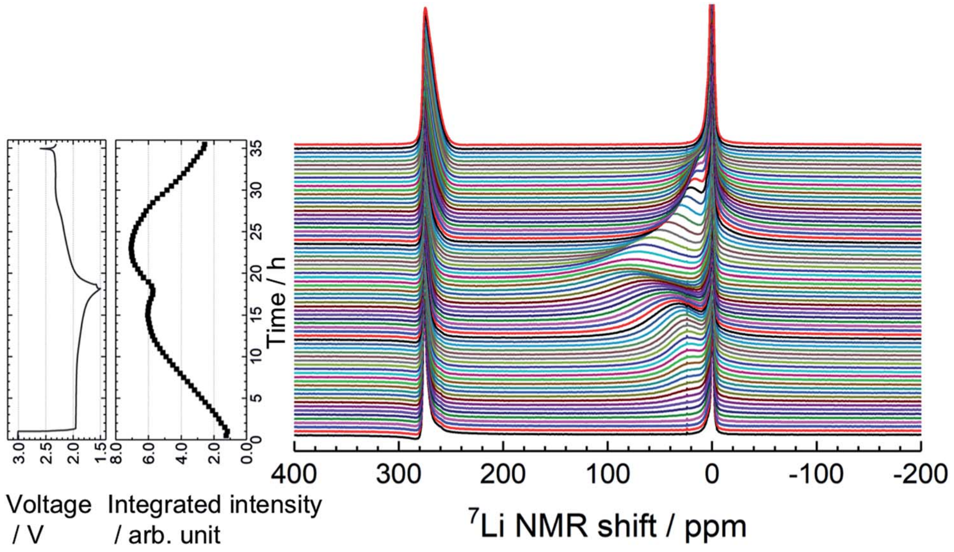

Fig. 3 Time evolution of operando ^{7}Li NMR spectra of the Li//a-VS_4 cell, along with the corresponding charge–discharge profile and integrated intensity plot of the a-Li_xVS_4 signal (including electrolyte signal). The spectra were accumulated for a flat laminate cell placed vertically in the center of coil.

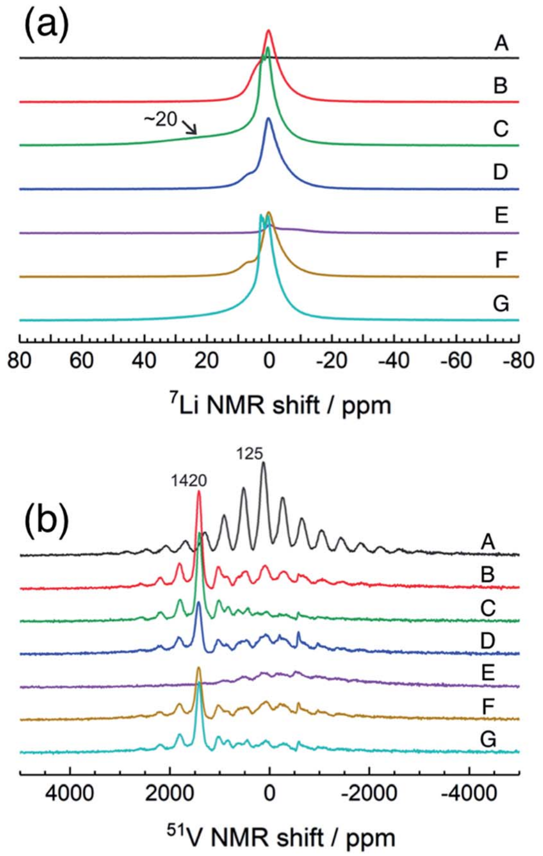

Fig. 4 ^{7}Li and ^{51}V MAS NMR spectra of a-VS_4 electrode samples disassembled at the points marked in Fig. 2.

structural disorder caused by back-transformation from the $[VS_4]^{3-}$ tetrahedral monomer to the one-dimensional chain-like structure, in which V–V spin-pairing may be partly ineffective and, in that case, the V^{4+} ions will be partially invisible in the ^{51}V MAS NMR spectrum. The recovery of the pristine structure was also confirmed by Raman spectra (Fig. S5†). In addition, a small peak was shown at −580 ppm in some spectra. A similar peak was identified in the previous study and tentatively ascribed to the V^{5+} ions with nearby V^{4+} ions.[27] However, we here attribute this signal to the $LiVO_3$ impurity phase (−573 ppm).[36]

Examination of these results gives essential information on the structure of pristine a-VS_4 and its changes during the lithiation/delithiation process. The local structure of a-VS_4 resembles that of c-VS_4: the pristine a-VS_4 consists of a one-dimensional chain-like structure with alternate short and long V–V distances, but long-range ordering is lost due to the positional disorder introduced by high-energy ball milling. The first Li insertion into a-VS_4 proceeds as a two-phase reaction. The lithiation of a-VS_4 to a-Li_3VS_4 involves drastic changes in local structure: the one-dimensional chains of V–V bonds and S–S disulfide bonds are broken, and $[VS_4]^{3-}$ tetrahedral monomers are formed. This reaction involves the oxidation of V ions as well as the reduction of S ions: the valence states of V^{4+} and S^- (or $[S_2]^{2-}$) in a-VS_4 changes to V^{5+} and S^{2-} in a-Li_3VS_4, respectively.[27] Further lithiation of a-Li_3VS_4 to a-$Li_{3+d'}VS_4$ causes partial reduction of the V valence state. The amorphous phase at 1.5 V (Li_5VS_4 composition) still includes a large amount of $[VS_4]^{3-}$ tetrahedral units. Information on the local structure around the paramagnetic V^{4+} and/or V^{3+} ions is not available from the ^{51}V NMR spectra. Theoretical calculations of the $Li_{3+d}VO_4$ model structures proposed the coexistence of tetrahedral and octahedral V sites in Li_5VO_4.[37] Recently, the V^{3+} ion in an octahedral environment was suggested in $Li_{3+d}VO_4$ based on the V K-edge XANES spectra.[38] Similar coordination change may be considered in a-$Li_{3+d'}VS_4$, and the V K-edge XANES spectrum of a-Li_xVS_4 provides supplementary information.[29] The conversion to elemental V does not occur within the potential window used in this study. The structure of a-$Li_{3+d'}VS_4$ changes reversibly to that of a-VS_4 during the delithiation process, but it necessitates drastic changes in the local environments of the V and S ions, leading to apparent voltage hysteresis in the charge–discharge profile. The structure of a-VS_4 after the 1st cycle delithiation is similar to that of the pristine material, but with significant local disorder. The tetrahedral structure phase completely disappeared and, therefore, the irreversible capacity of 65 mA h g^{-1} may be associated with the formation of solid-electrolyte interphases (SEI) involving electrolyte decomposition. The XPS spectra of the lithiated and delithiated samples showed the deposition of organic components on the electrode surface, which makes it difficult to evaluate the valence states of V and S ions in these samples (not shown). The present study indicates that the lithiation/delithiation process of a-VS_4 is basically the same as that previously reported for c-VS_4:[27] lithium insertion into c-VS_4 results in amorphous phases such as a-Li_3VS_4 and a-$Li_{3+d'}VS_4$, which then revert to a-VS_4 after the initial charge–discharge cycling. Recently, a similar lithium insertion/extraction behavior has been proposed for amorphous TiS_4 (a-TiS_4):[39] the structural changes of a-TiS_4 toward a-Li_4TiS_4 involve the breaking of S–S disulfide bonds and a gradual decrease in the average coordination number of Ti ions. These results indicate that the structural changes of sulfur-rich TM sulfides during Li insertion/extraction are related to the changes in both the bonding nature of sulfide species and the coordination number of TM ions. The amorphous host structure can accommodate these modifications, which is not topotactic as in crystalline electrode materials. From the viewpoint of the charge compensation mechanism, stable cation and anion redox reactions are easily available for amorphous sulfur-rich TM sulfide electrodes, which is a key factor for stable high capacity batteries.[40]

4. Conclusions

The amorphous VS_4 (a-VS_4) was mechanochemically prepared from crystalline VS_4 (c-VS_4), and its structural changes during the lithiation/delithiation process were investigated using solid-state NMR spectroscopy. ^{51}V MAS NMR measurements gave extensive information on the amorphous host structures and valence states of the pristine a-VS_4 and its lithiated materials. The local structure of a-VS_4 resembles that of c-VS_4, which consists of a one-dimensional chain structure with Peierls distortion. The lithiation/delithiation mechanism of a-VS_4 is expected to be the same as that of c-VS_4, and lithiated a-Li_xVS_4 materials are amorphous during charge–discharge cycling. The local structure of a-VS_4 changes drastically when Li ions are inserted. In the amorphous Li_3VS_4 phase (a-Li_3VS_4), the one-dimensional chain structure is decomposed to an isolated $[VS_4]^{3-}$ structure with interstitial Li ions, which involves a unique internal redox process between V and S ions. Further Li insertion into a-$Li_{3+d'}VS_4$ is associated with the reduction of V ions. After the 1st cycle, a-VS_4 recovers to a highly disordered chain-like structure. Stable Li insertion/extraction is feasible in between a-VS_4 and a-Li_5VS_4 with a high capacity of ~700 mA h g^{-1} using a narrow potential window between 1.5 and 2.6 V. Amorphous sulfur-rich TM sulfides can accommodate reversible changes in both the bonding nature of sulfide species and the coordination number of TM ions, which is a source of stable cation and anion redox reactions, leading to high charge–discharge capacities.

Conflicts of interest

There are no conflicts to declare.

Acknowledgements

This work was supported by the Research and Development Initiative for Scientific Innovation of New Generation Batteries 2 (RISING2) funded by the New Energy and Industrial Technology Development Organization (NEDO), Japan (Project code: P16001). The authors thank Mr Takashi Moroishi for his support in the sample preparation and NMR measurements.

References

1 X. Ji and L. F. Nazar, *J. Mater. Chem.*, 2010, **20**, 9821–9826.
2 R. D. Rauh, F. S. Shuker, J. M. Marston and S. B. Brummer, *J. Inorg. Nucl. Chem.*, 1977, **39**, 1761–1766.
3 Q. Liu, D. Mu, B. Wu, L. Wang, L. Gai and F. Wu, *RSC Adv.*, 2017, **7**, 33373–33377.
4 C. Liang, N. J. Dudney and J. Y. Howe, *Chem. Mater.*, 2009, **21**, 4724–4730.
5 X. Ji, K. T. Lee and L. F. Nazar, *Nat. Mater.*, 2009, **8**, 500–506.
6 G. Zheng, Q. Zhang, J. J. Cha, Y. Yang, W. Li, Z. W. She and Y. Cui, *Nano Lett.*, 2013, **13**, 1265–1270.
7 J. R. Dahn and R. R. Haering, *Mater. Res. Bull.*, 1979, **14**, 1259–1262.
8 J. R. Dahn, W. R. McKinnon, R. R. Haering, W. J. L. Buyers and B. M. Powell, *Can. J. Phys.*, 1980, **58**, 207–213.
9 S. Kostov, M. denBoer, E. Strauss, D. Golodnitsky, S. G. Greenbaum and E. Peled, *J. Power Sources*, 1999, **81–82**, 709–714.
10 Y. Shao-Horn, S. Osmialowski and Q. C. Horn, *J. Electrochem. Soc.*, 2002, **149**, A1547–A1555.
11 C. Feng, J. Ma, H. Li, R. Zeng, Z. Guo and H. Liu, *Mater. Res. Bull.*, 2009, **44**, 1811–1815.
12 G. Du, Z. Guo, S. Wang, R. Zeng, Z. Chen and H. Liu, *Chem. Commun.*, 2010, **46**, 1106–1108.
13 N. Sharma, G. Du, A. J. Studer, Z. Guo and V. K. Peterson, *Solid State Ionics*, 2011, **199–200**, 37–43.
14 X. Xu, W. Liu, Y. Kim and J. Cho, *Nano Today*, 2014, **9**, 604–630.
15 M. M. Butala, M. Mayo, V. V. T. Doan-Nguyen, M. A. Lumley, C. Göbel, K. M. Wiaderek, O. J. Borkiewicz, K. W. Chapman, P. J. Chupas, M. Balasubramanian, G. Laurita, S. Britto, A. J. Morris, C. P. Grey and R. Seshadri, *Chem. Mater.*, 2017, **29**, 3070–3082.
16 L. Zhang, D. Sun, J. Kang, H.-T. Wang, S.-H. Hsieh, W.-F. Pong, H. A. Bechtel, J. Feng, L.-W. Wang, E. J. Cairns and J. Guo, *Nano Lett.*, 2018, **18**, 4506–4515.

17 A. Sakuda, N. Taguchi, T. Takeuchi, H. Kobayashi, H. Sakaebe, K. Tatsumi and Z. Ogumi, *Electrochem. Commun.*, 2013, **31**, 71–75.

18 A. Sakuda, T. Takeuchi, K. Okamura, H. Kobayashi, H. Sakaebe, K. Tatsumi and Z. Ogumi, *Sci. Rep.*, 2014, **4**, 4883.

19 A. Sakuda, N. Taguchi, T. Takeuchi, H. Kobayashi, H. Sakaebe, K. Tatsumi and Z. Ogumi, *ECS Electrochem. Lett.*, 2014, **3**, A79–A81.

20 T. Matsuyama, A. Hayashi, T. Ozaki, S. Mori and M. Tatsumisago, *J. Mater. Chem. A*, 2015, **3**, 14142–14147.

21 T. Takeuchi, H. Kageyama, K. Nakanishi, M. Ogawa, T. Ohta, A. Sakuda, H. Sakaebe, H. Kobayashi and Z. Ogumi, *J. Electrochem. Soc.*, 2015, **162**, A1745–A1750.

22 A. Sakuda, T. Takeuchi, M. Shikano, K. Ohara, K. Fukuda, Y. Uchimoto, Z. Ogumi, H. Kobayashi and H. Sakaebe, *J. Ceram. Soc. Jpn.*, 2017, **125**, 268–271.

23 X. Wang, K. Du, C. Wang, L. Ma, B. Zhao, J. Yang, M. Li, X.-X. Zhang, M. Xue and J. Chen, *ACS Appl. Mater. Interfaces*, 2017, **9**, 38606–38611.

24 R. Allmann, I. Baumann, A. Kutoglu, H. Rosch and E. Hellner, *Sci. Nat.*, 1964, **51**, 263–264.

25 C. S. Rout, B.-H. Kim, X. Xu, J. Yang, H. Y. Jeong, D. Odkhuu, N. Park, J. Cho and H. S. Shin, *J. Am. Chem. Soc.*, 2013, **135**, 8720–8725.

26 X. Xu, S. Jeong, C. S. Rout, P. Oh, M. Ko, H. Kim, M. G. Kim, R. Cao, H. S. Shin and J. Cho, *J. Mater. Chem. A*, 2014, **2**, 10847–10853.

27 S. Britto, M. Leskes, X. Hua, C.-A. Herbert, H. S. Shin, S. Clarke, O. Borkiewicz, K. W. Chapman, R. Seshadri, J. Cho and C. P. Grey, *J. Am. Chem. Soc.*, 2015, **137**, 8499–8508.

28 K. K. A. Sakuda, T. Takeuchi, H. Sakaebe, H. Kobayashi, H. Kageyama, T. Kawaguchi, H. Kiuchi, K. Nakanishi, M. Yoshimura, T. Ohta, T. Fukunaga and E. Matsubara, *Solid State Ionics*, 2018, **323**, 32–36.

29 K. Koganei, A. Sakuda, T. Takeuchi, H. Sakaebe, H. Kobayashi, H. Kiuchi, T. Fukunaga and E. Matsubara, *69th Annual Meeting of the International Society of Electrochemistry*, S06a-028 (abstract), 2018.

30 M. N. Kozlova, Y. V. Mironov, E. D. Grayfer, A. I. Smolentsev, V. I. Zaikovskii, N. A. Nebogatikova, T. Y. Podlipskaya and V. E. Fedorov, *Chem.–Eur. J.*, 2015, **21**, 4639–4645.

31 M. S. Weimer, R. F. McCarthy, J. D. Emery, M. J. Bedzyk, F. G. Sen, A. Kinaci, M. K. Y. Chan, A. S. Hock and A. B. F. Martinson, *Chem. Mater.*, 2017, **29**, 2864–2873.

32 M. Wang, L. Fan, Y. Qiu, D. Chen, X. Wu, C. Zhao, J. Cheng, Y. Wang, N. Zhang and K. Sun, *J. Mater. Chem. A*, 2018, **6**, 11694–11699.

33 R. St, C. Smart, W. M. Skinner and A. R. Gerson, *Surf. Interface Anal.*, 1999, **28**, 101–105.

34 K. Shimoda, M. Murakami, T. Takeuchi, T. Matsunaga, Y. Ukyo, H. Sakaebe, H. Kobayashi and E. Matsubara, *J. Power Sources*, 2018, **398**, 67–74.

35 P. Duerichen and W. Bensch, *Eur. J. Solid State Inorg. Chem.*, 1996, **33**, 309–320.

36 J. Skibsted, C. J. H. Jacobsen and H. J. Jakobsen, *Inorg. Chem.*, 1998, **37**, 3083–3092.

37 M. E. Arroyo-de Dompablo, P. Tartaj, J. M. Amarilla and U. Amador, *Chem. Mater.*, 2016, **28**, 5643–5651.

38 P. Rozier, E. Iwama, N. Nishio, K. Baba, K. Matsumura, K. Kisu, J. Miyamoto, W. Naoi, Y. Orikasa, P. Simon and K. Naoi, *Chem. Mater.*, 2018, **30**, 4926–4934.

39 A. Sakuda, K. Ohara, K. Fukuda, K. Nakanishi, T. Kawaguchi, H. Arai, Y. Uchimoto, T. Ohta, E. Matsubara, Z. Ogumi, T. Okumura, H. Kobayashi, H. Kageyama, M. Shikano, H. Sakaebe and T. Takeuchi, *J. Am. Chem. Soc.*, 2017, **139**, 8796–8799.

40 E. D. Grayfer, E. M. Pazhetnov, M. N. Kozlova, S. B. Artemkina and V. E. Fedorov, *ChemSusChem*, 2017, **10**, 4805–4811.